Electronic Supplementary Information for:

Large breathing effect induced by water sorption in a remarkably stable nonporous cyanide-bridged coordination polymer

Michał Magott,[a,*] Bartłomiej Gaweł,[b] Marcin Sarewicz,[c] Mateusz Reczyński,[a] Karolina Ogorzały,[a] Wacław Makowski,[a] Dawid Pinkowicz[a,*]

[a] *Faculty of Chemistry, Jagiellonian University, Gronostajowa 2, 30-387 Kraków, Poland*

[b] *Department of Materials Science and Engineering, Norwegian University of Science and Technology (NTNU), 7491 Trondheim, Norway*

[c] *Department of Molecular Biophysics, Faculty of Biochemistry, Biophysics and Biotechnology, Jagiellonian University, Gronostajowa 7, 30-387 Kraków, Poland*

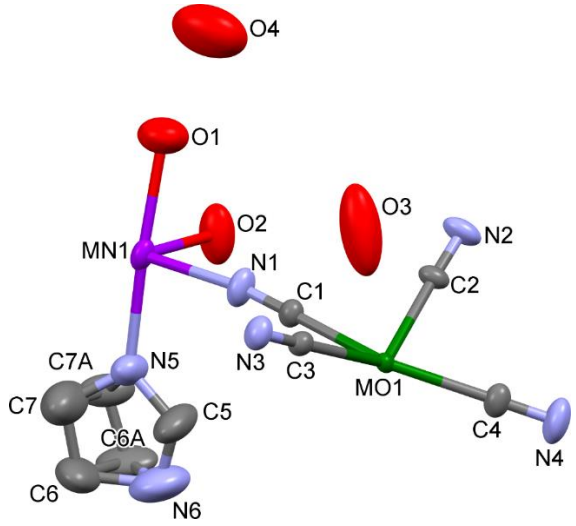

Figure S1. The asymmetric unit of **1Mn·8H$_2$O**. Centroids are depicted at the 50% probability level for a room temperature structure.

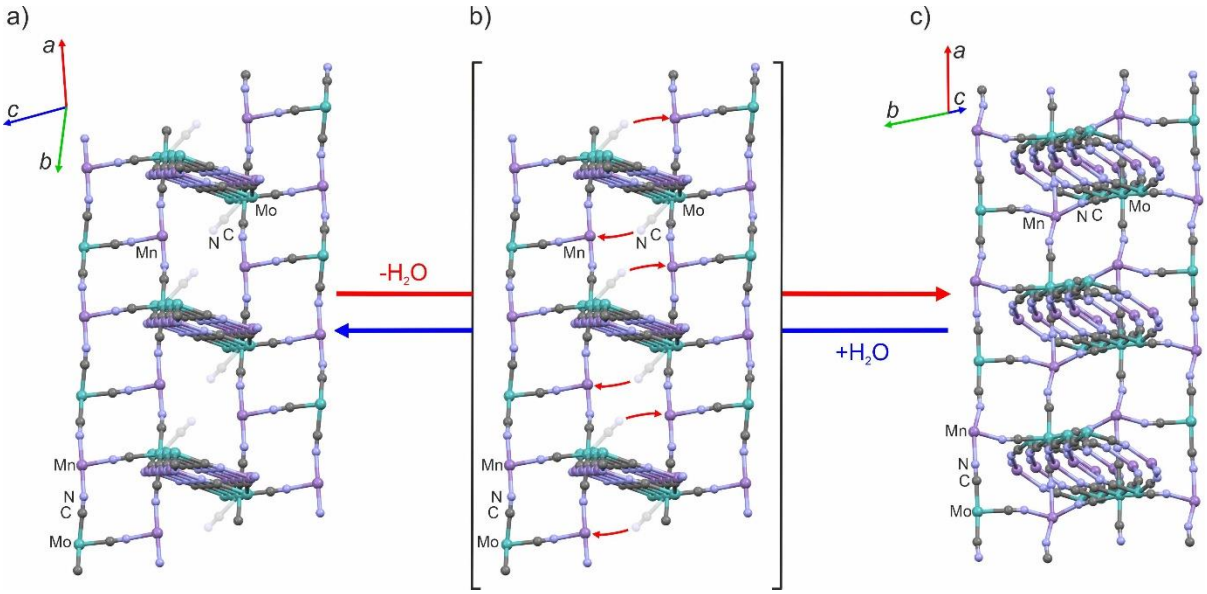

Figure S2. Structural diagrams similar to those in Figure 2 (main text) with colour coded atoms, showing the change of the cyanide bridging pattern in the last step of the dehydration of **1Mn·2H$_2$O** (a) accompanied by the additional CN-bridge formation (b) which finally yields anhydrous **1Mn** (c). The initial "crossed-ladders" CN-bridged skeleton of **1Mn·2H$_2$O** (a) transforms into a "ladders-crossing-square-grids" CN-bridged scaffold of **1Mn** due to the merging of one type of ladder motifs into square-grid motifs through the formation of the additional CN-bridge. See Figure 2 in the main text for a better visualization of the bridging pattern.

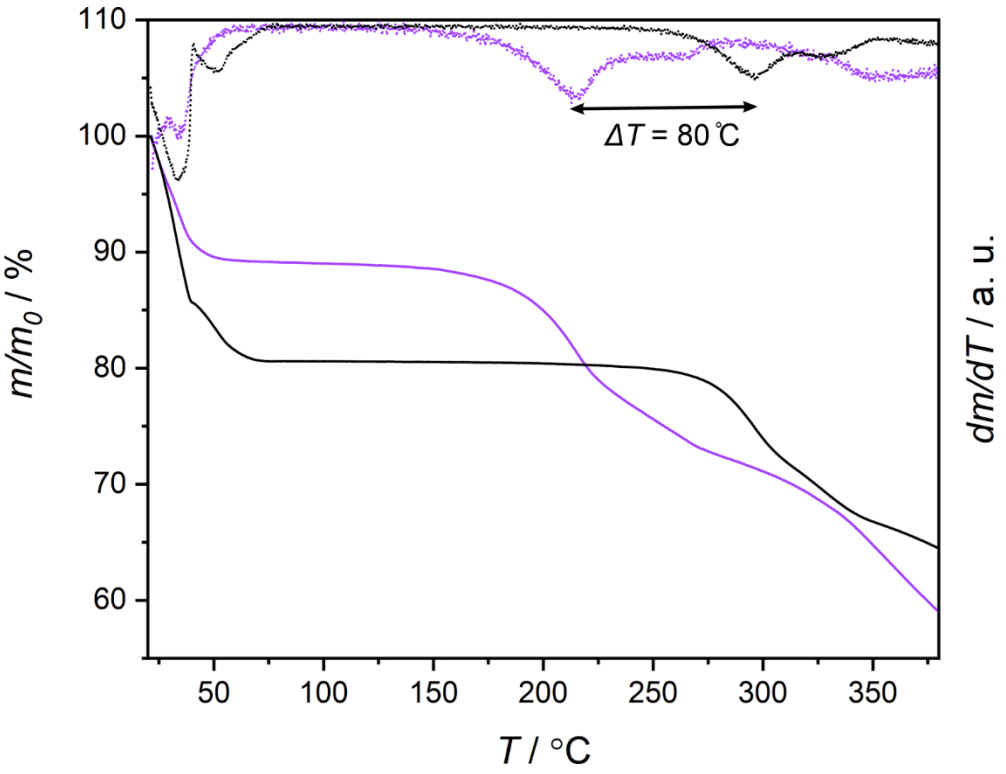

Figure S3. Thermogravimetric analysis for **1Mn·8H$_2$O** (black) and **2Cd·8H$_2$O** (purple). Solid lines denote relative mass change, while dotted lines represent its derivative in respect to temperature.

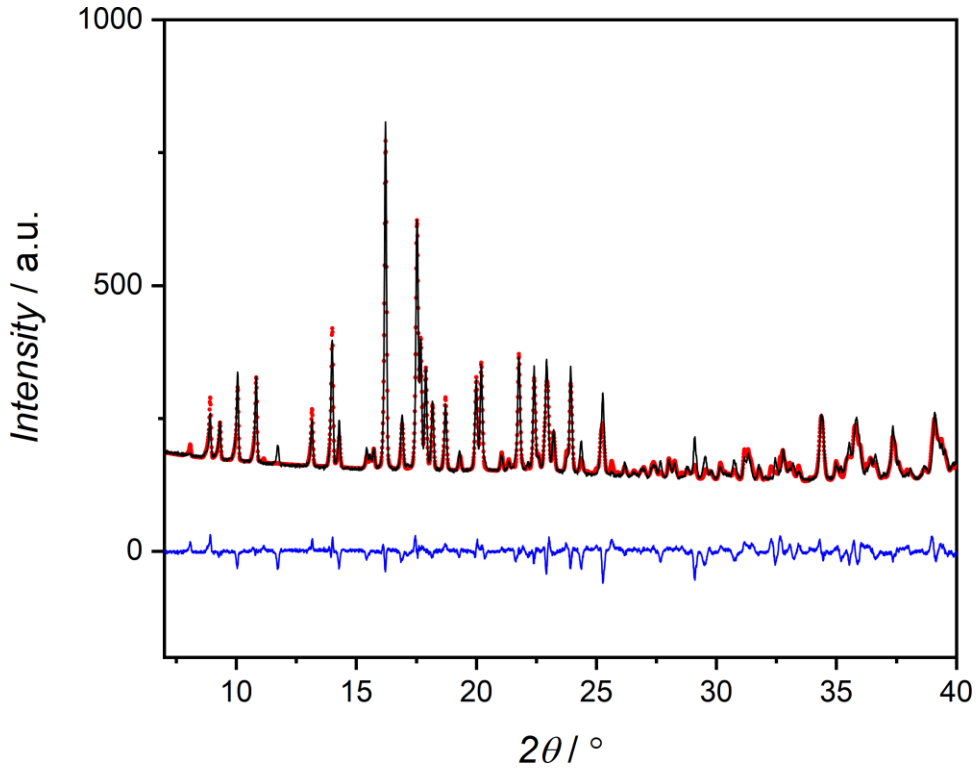

Figure S4. The calculated (red points) and observed (black line) PXRD patterns for **1Mn·3H$_2$O**. The blue line presents the difference between the calculated and experimental data.

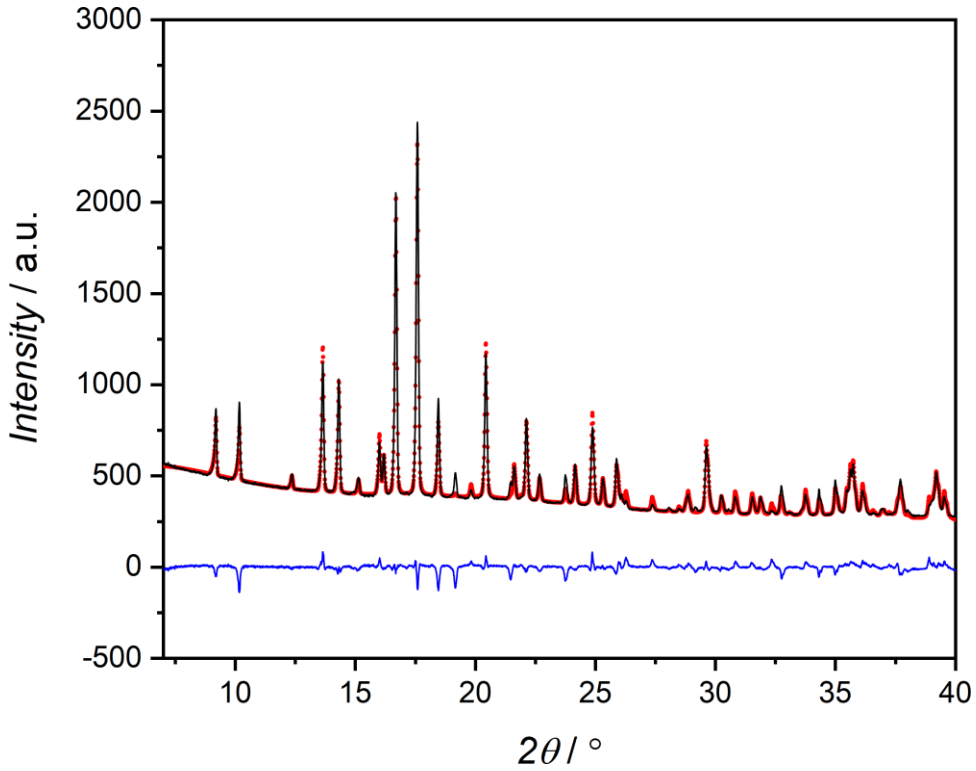

Figure S5. The calculated (red points) and observed (black line) PXRD patterns for **1Mn·2H$_2$O**. The blue line presents the difference between the calculated and experimental data.

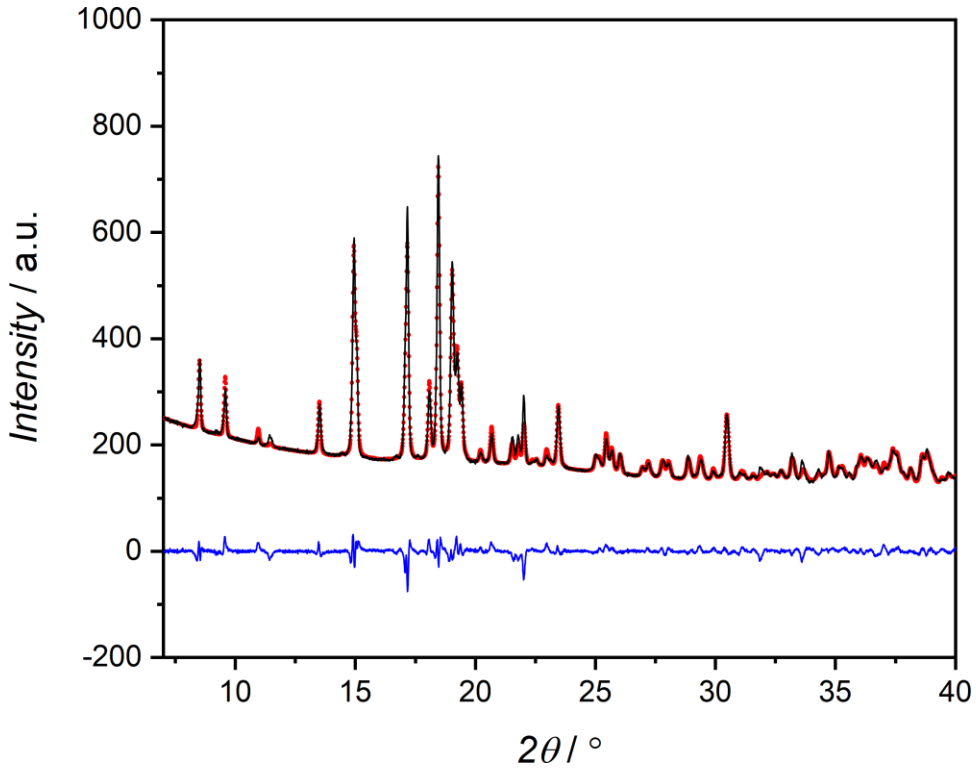

Figure S6. The calculated (red points) and observed (black line) PXRD patterns for **1Mn**. The blue line presents the difference between the calculated and experimental data.

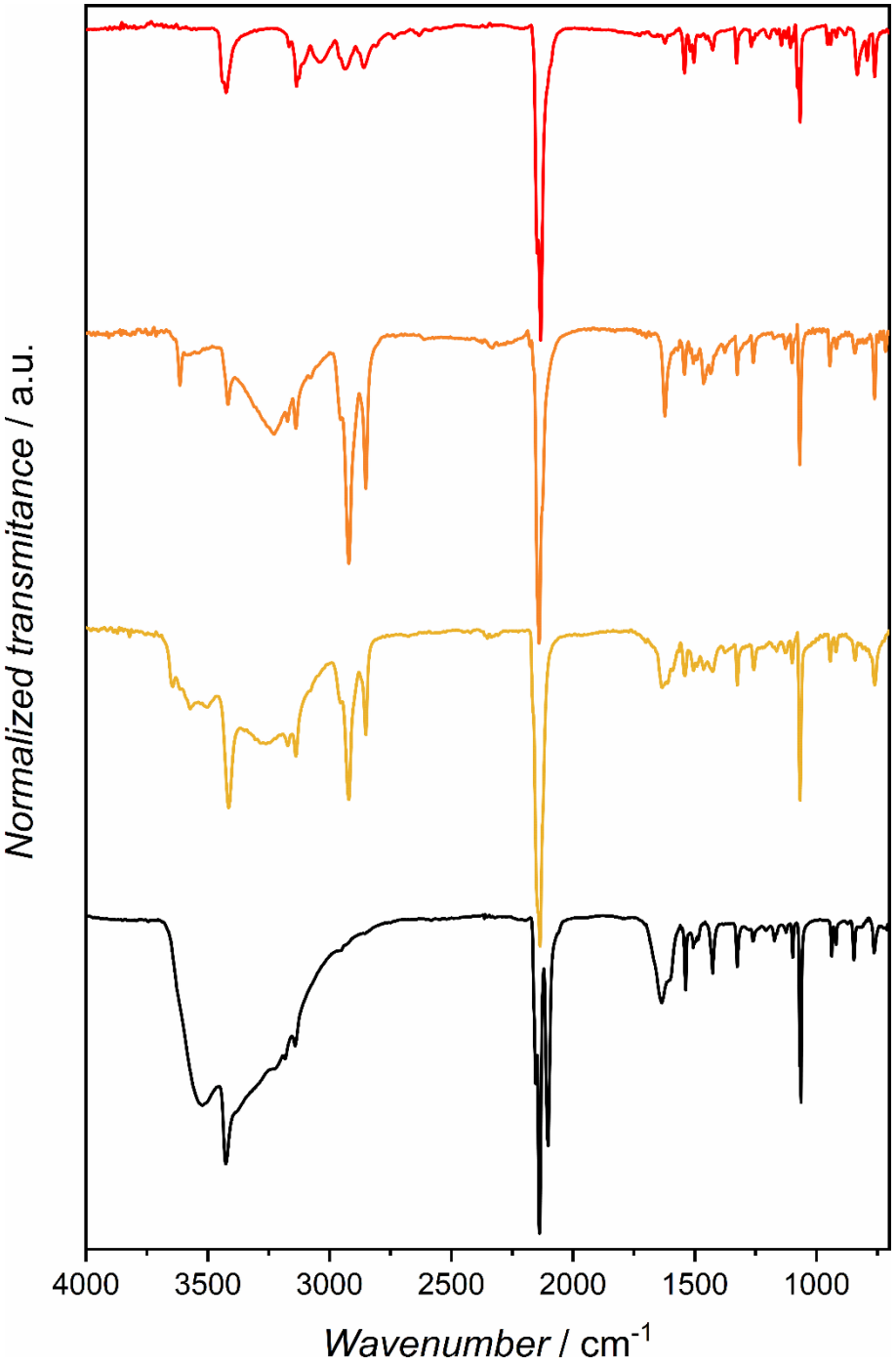

Figure S7. IR spectra for **1Mn·8H$_2$O** (black), **1Mn·3H$_2$O** (yellow), **1Mn·2H$_2$O** (orange), and **1Mn** (red).

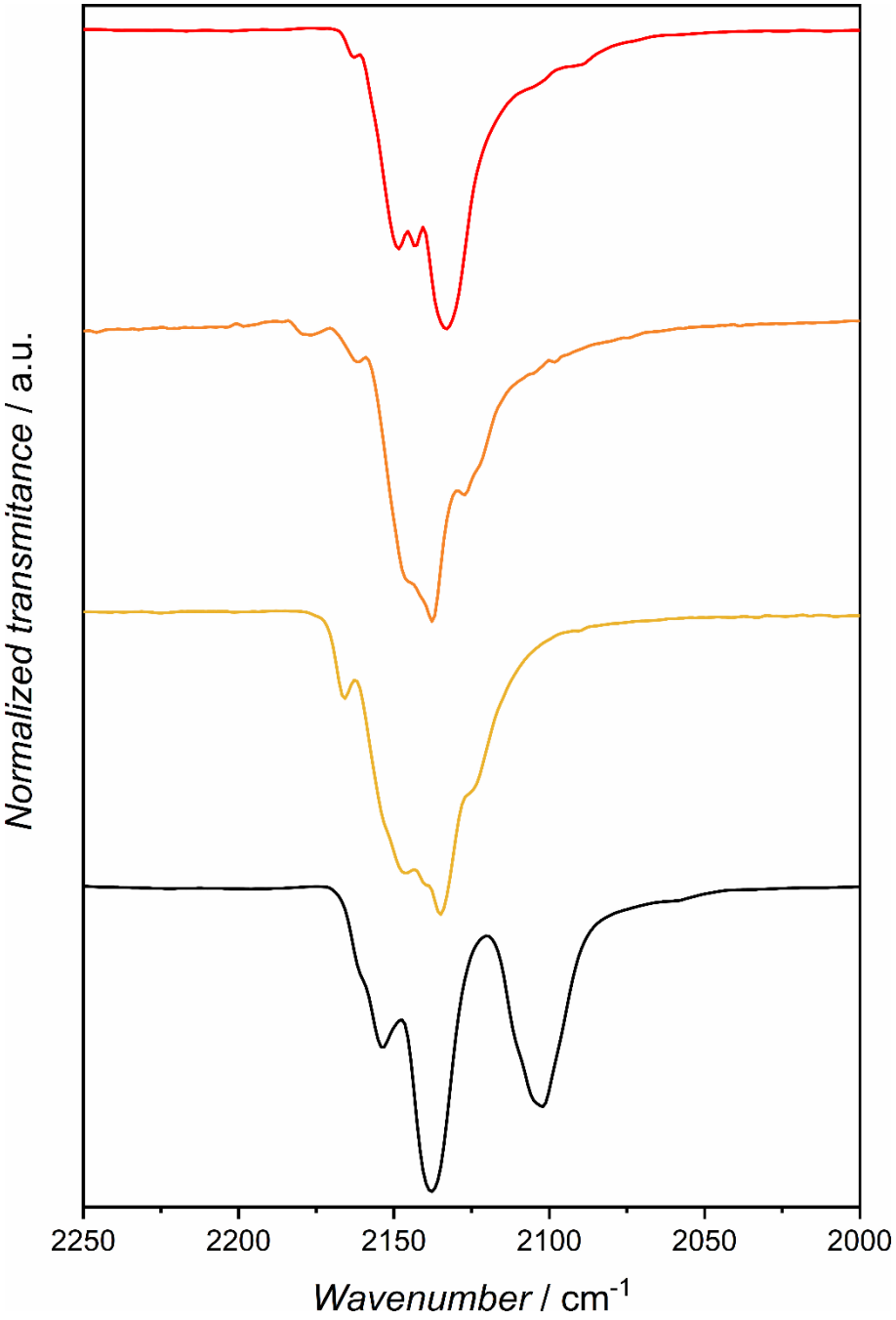

Figure S8. Cyanide stretching region IR spectra for **1Mn·8H₂O** (black), **1Mn·3H₂O** (yellow), **1Mn·2H₂O** (orange), and **1Mn** (red).

Description of the IR spectroscopy results

The most pronounced changes observed in the IR spectra depicted in Figure S7 include the disappearance of the broad O-H stretching band in the 3000-3700 cm^{-1} range and the decrease in the intensity of the 1620-1640 cm^{-1} O-H bending vibration upon transition from **1Mn·8H$_2$O** to **1Mn** The stepwise disappearance of the characteristic water vibration bands is in compliance with the quantitative measurements of water content in this phases (DVS and QE-TPDA). Apart from the O-H bending band, the fingerprint region of the spectra is dominated by the characteristic bands of imidazole ligands, which remain almost unchanged for all the phases and therefore confirm that its role as a capping ligand is largely unaffected by the water desorption. The most pronounced changes regarding imidazole molecule is the variation of the N-H and C-H band intensity in the 2850-3600 cm^{-1} range, which may be caused by the changes in hydrogen bonding and/or imidazole molecule arrangement in the crystal lattice. Significant changes are also visible in the cyanide stretching region presented in Figure S8, with distinct changes of the fine structure of the band localized at 2140 cm^{-1}. Additionally, in the first step of dehydration (from **1Mn·8H$_2$O** to **1Mn·3H$_2$O**) the separate band at 2100 cm^{-1} disappears and thus we hypothesize that this feature may originate from the hydrogen bonding between the terminal CN^- ligands of the octacyanomolybdate(IV) moieties and the crystallization water molecules (as the latter are absent in all other phases). No further conclusions could be drawn from the cyanide stretching vibration region, especially the changes in the 2200-2000 cm^{-1} region between **1Mn·2H$_2$O** and **1Mn** are inconclusive regarding the formation of an additional cyanide bridge at this step.

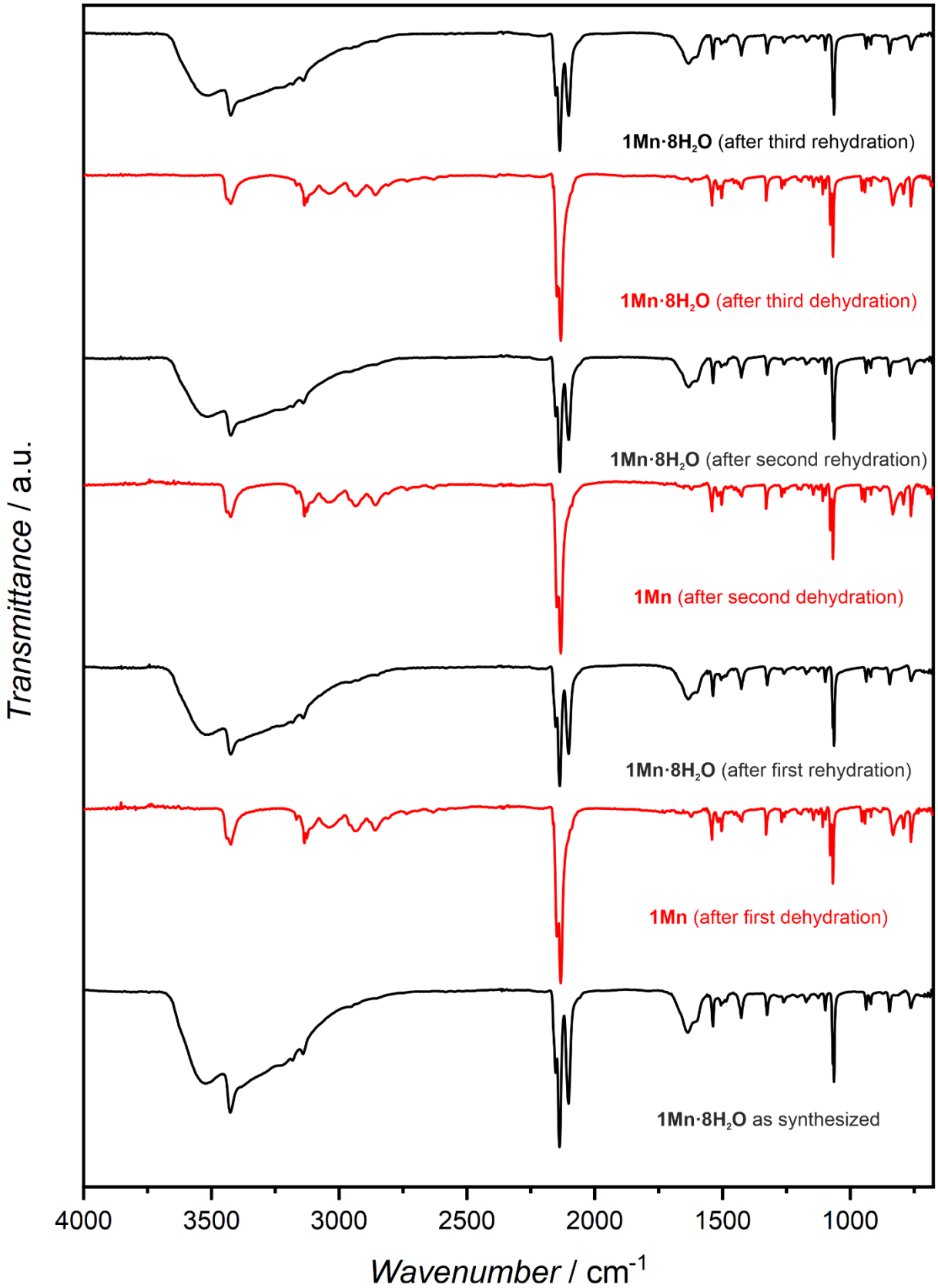

Figure S9. IR spectra recorded for **1Mn·8H$_2$O** during three consecutive full dehydration (red lines, 0% RH, 353 K) / rehydration cycles (black lines, >95% RH, 298 K).

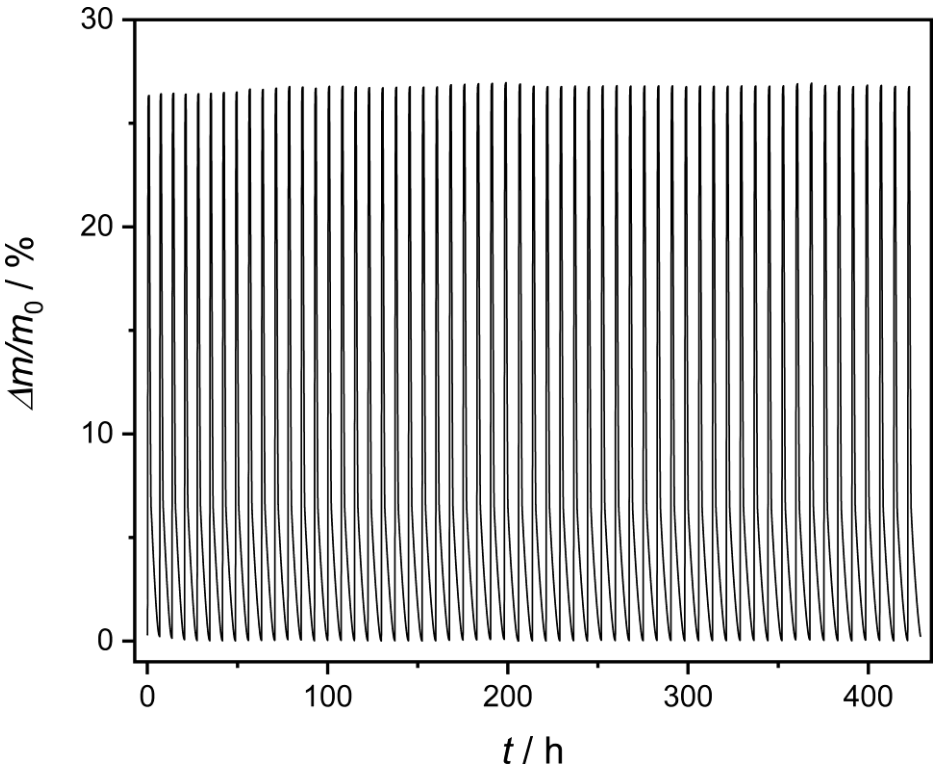

Figure S10. Water cycling stability test for 57 adsorption(p/p_0 = 0.95)–desorption(p/p_0 = 0) cycles conducted on **1Mn** at 298 K.

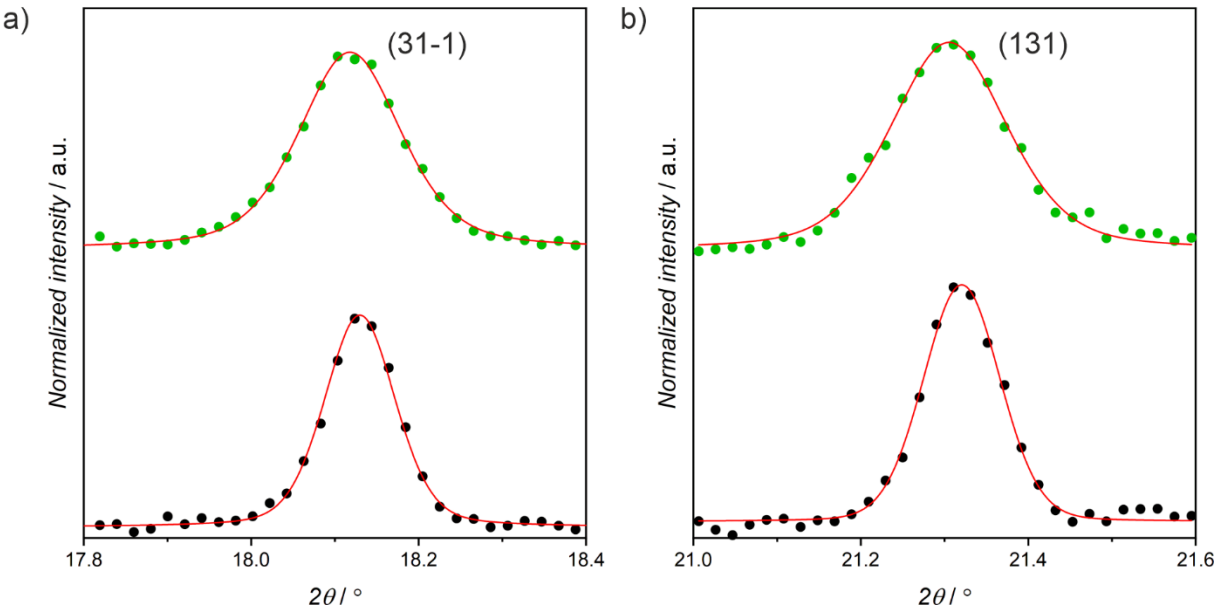

Figure S11. Comparison of peak broadening for **1Mn·8H₂O** in the pristine state (black points) and after 58 dehydration-rehydration cycles (green points). The red line shows best fits to the pseudo-Voigt line profile $y = y_0 + A\left[\eta \cdot \frac{1}{\pi} \cdot \frac{\left(\frac{\Gamma}{2}\right)}{(x-x_0)^2+\left(\frac{\Gamma}{2}\right)^2} + (1-\eta) \cdot \sqrt{\frac{\ln 2}{\pi}} \cdot \frac{2}{\Gamma} \cdot e^{\frac{4 \ln 2 (x-x_0)^2}{\Gamma^2}}\right]$ with the following FWHM parameters: a) Γ = 0.099(2) (bottom) and Γ = 0.144(3) (top); b) Γ = 0.108(3) (bottom) and Γ = 0.164(6) (top).

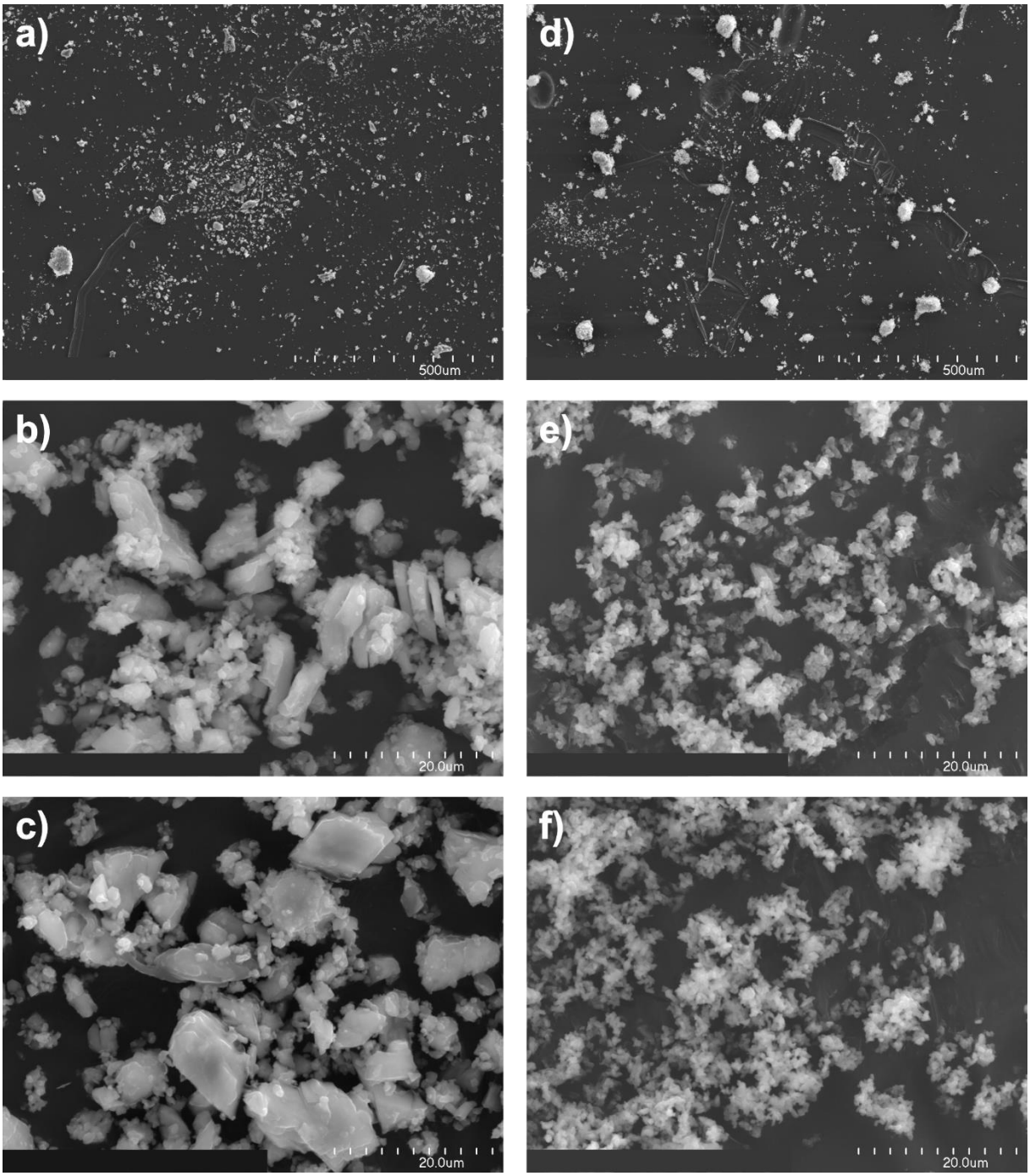

Figure S12. SEM pictures of **1Mn·8H$_2$O** before (a-c) and after (d-f) 58 dehydration-rehydration cycles at room temperature. Initial sample was ground in the agate mortar and dried in vacuum before SEM photographs were taken.

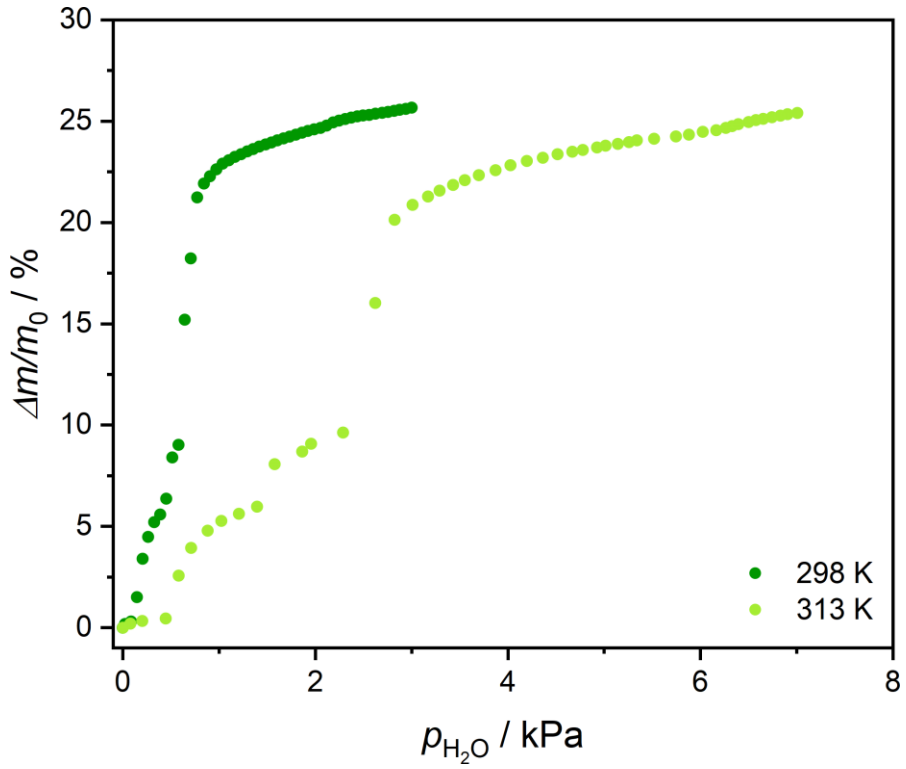

Figure S13. Water adsorption isotherms recorded for **1Mn** at 298 K (dark green) and 313 K (light green). *X*-axis presents absolute values of water vapor pressure.

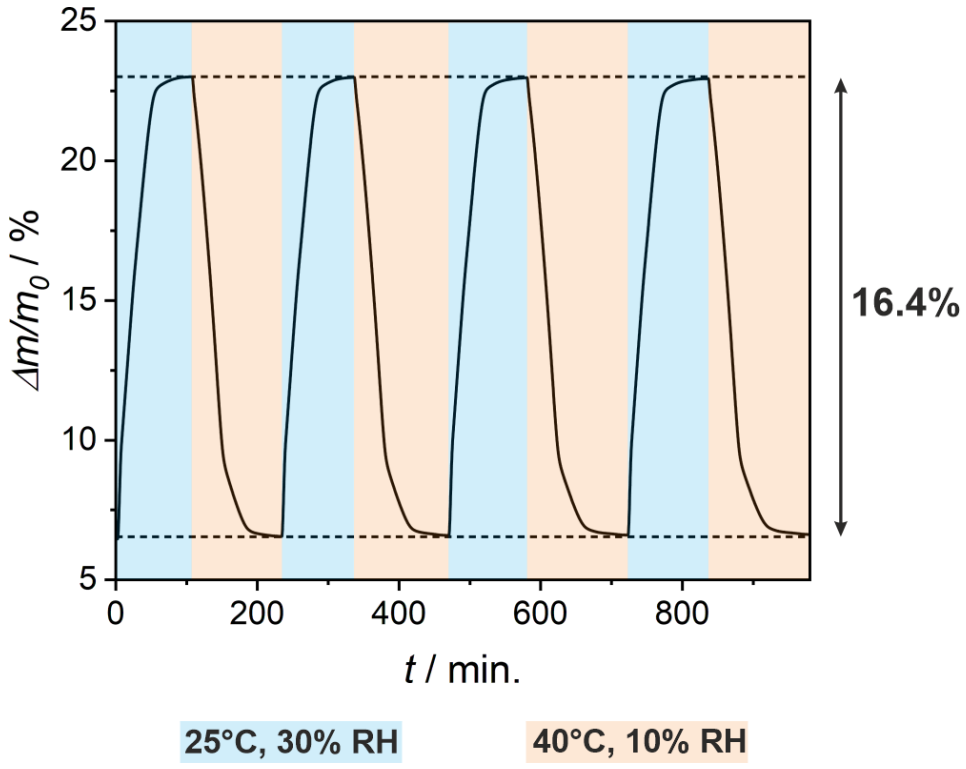

Figure S14. Dynamic vapor sorption measurement of **1Mn** during cycling between 25 °C (30% RH) and 40 °C (10% RH)

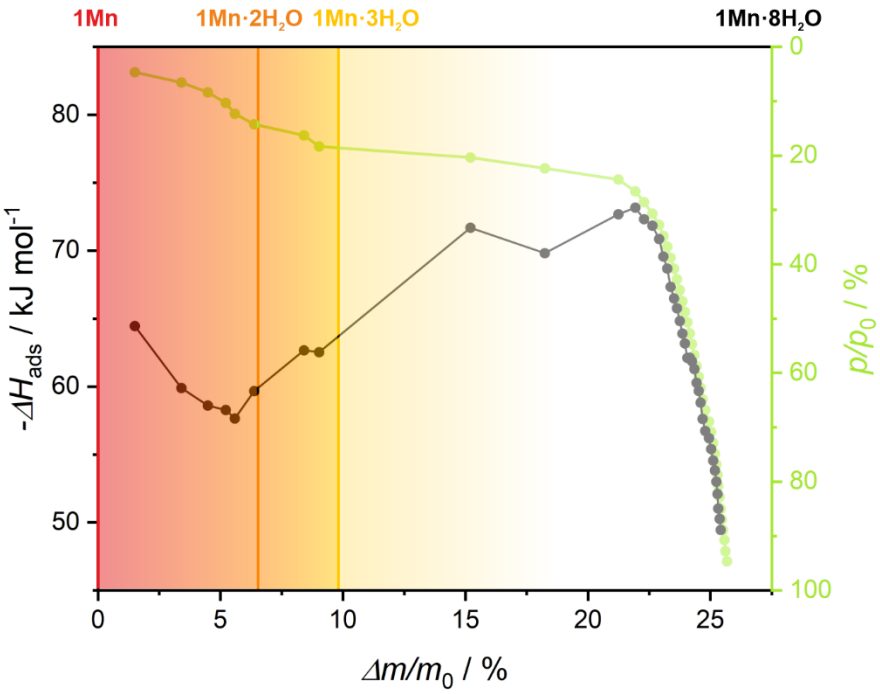

Figure S15. Isosteric enthalpies of water adsorption for **1Mn** calculated using the van't Hoff equation (black points) and water adsorption isotherm at 298 K (green points). Solid lines are guides for the eye.

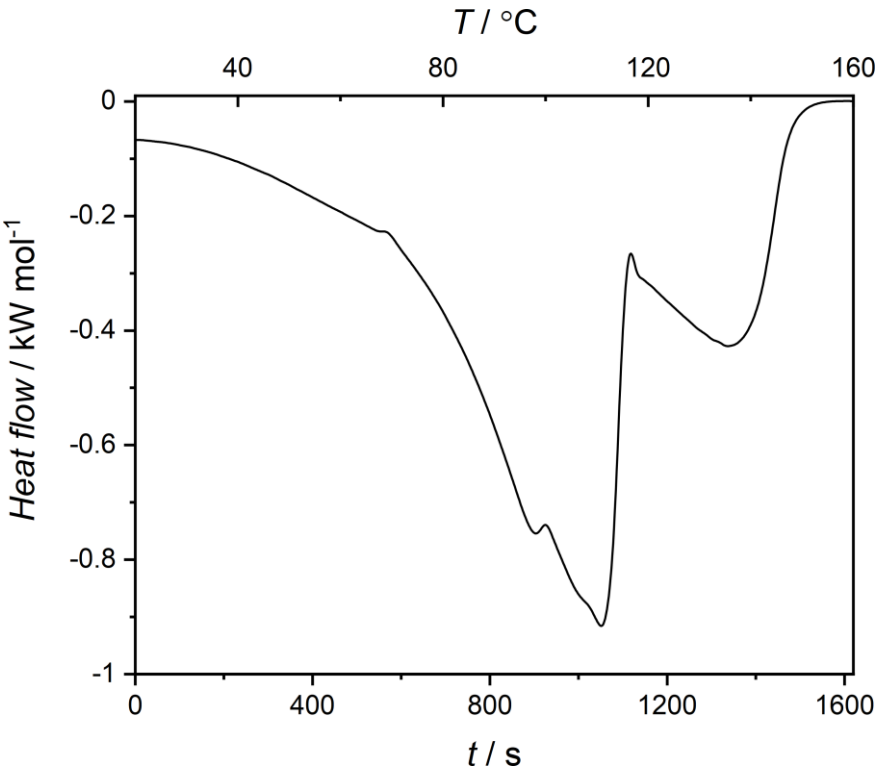

Figure S16. Differential scanning calorimetry (DSC) curve obtained for **1Mn·8H₂O** at the heating rate of 5 °C/min.

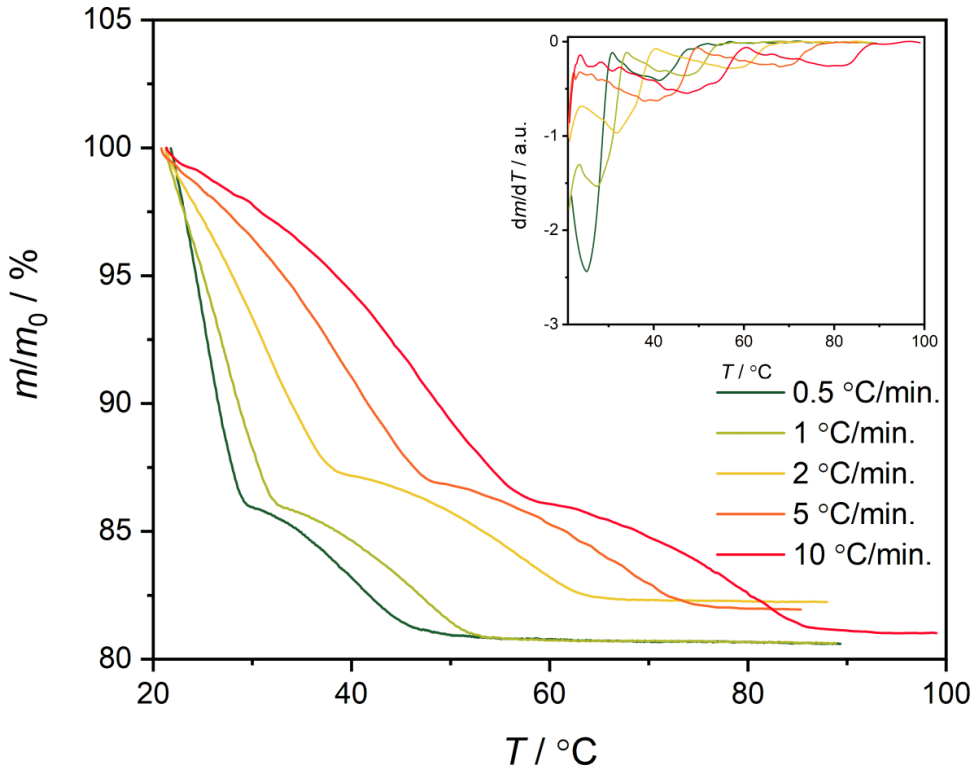

Figure S17. Thermogravimetric analysis for **1Mn·8H$_2$O** recorded at different heating rates. The difference in observed mass changes is the result of partial sample dehydration before measurement starts. Inset shows a numerical derivative of the data present on the main graph.

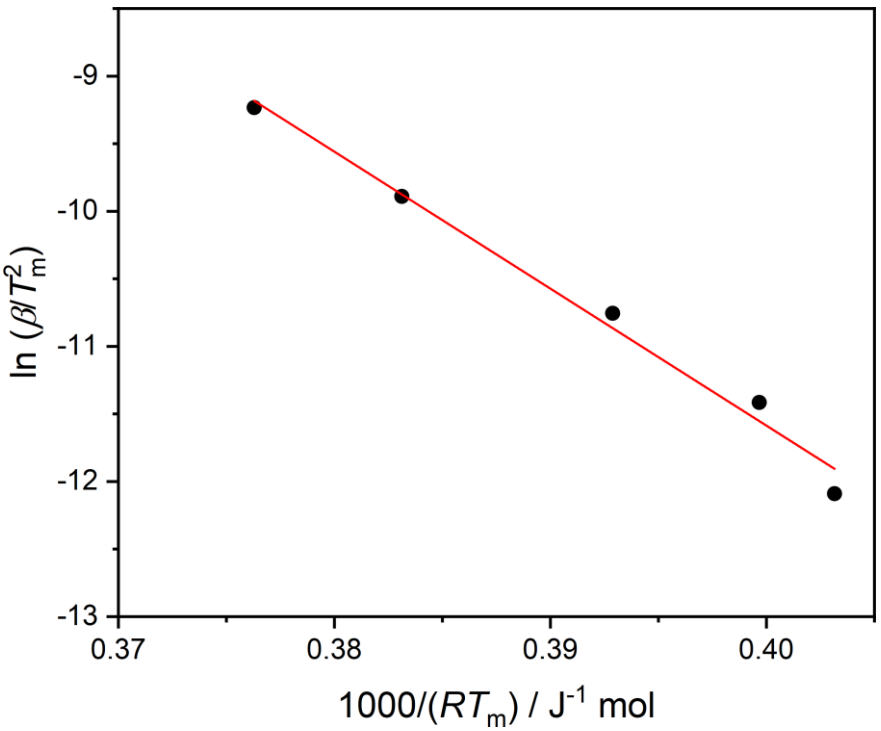

Figure S18. Kissinger plot for calculation of water desorption activation energy in the first step of dehydration (**1Mn·8H₂O → 1Mn·2H₂O**). Experimental points are depicted as black circles, while the red line represents the best fit (R^2 = 98.7%). B – heating rate, T_m – the temperature at the maximum rate of mass change (d*m*/d*T*).

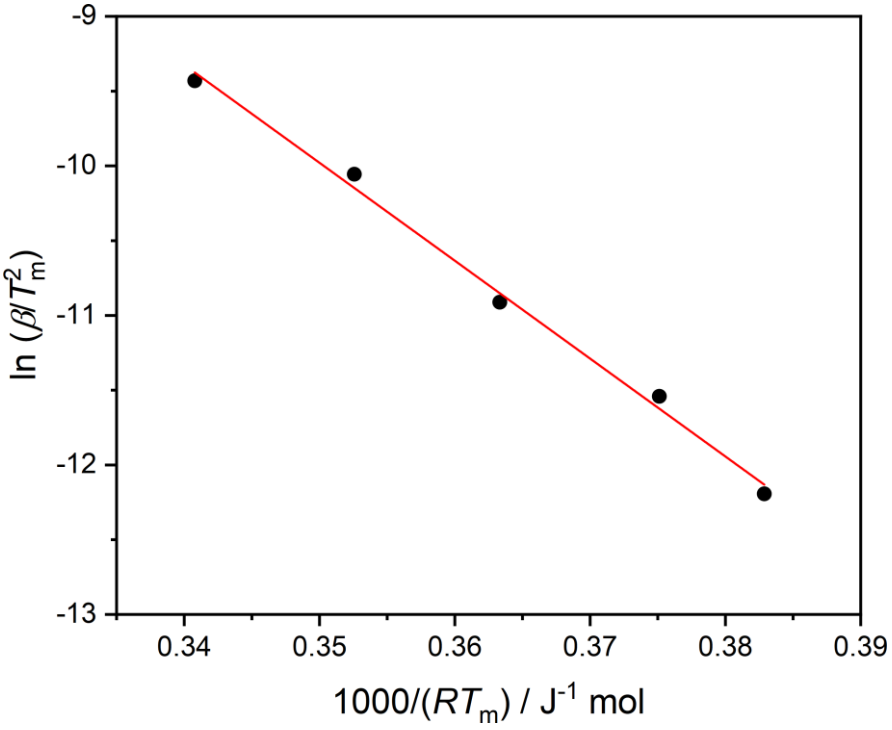

Figure S19. Kissinger plot for calculation of water desorption activation energy in the second step of dehydration (**1Mn·2H₂O → 1Mn**). Experimental points are depicted as black circles, while the red line represents the best fit (R^2 = 99.5%). B – heating rate, T_m – the temperature at the maximum rate of mass change (d*m*/d*T*).

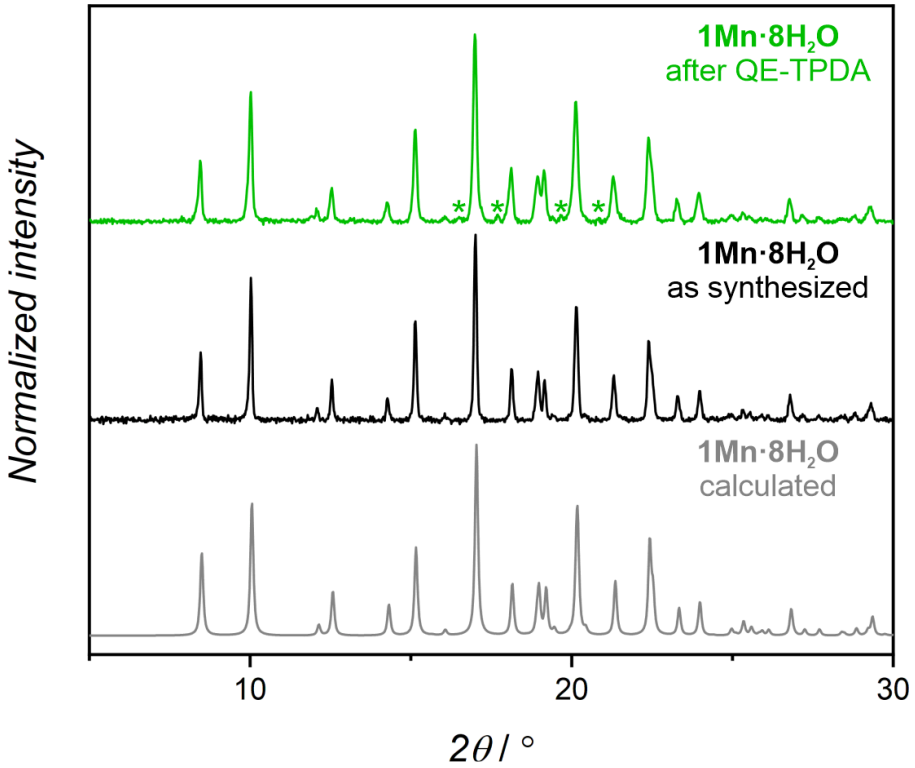

Figure S20. Powder X-ray diffraction patterns simulated from the single-crystal structure of **1Mn·8H$_2$O** (bottom), obtained for a pristine sample (middle) and obtained for the sample after QE-TPDA experiment (top).

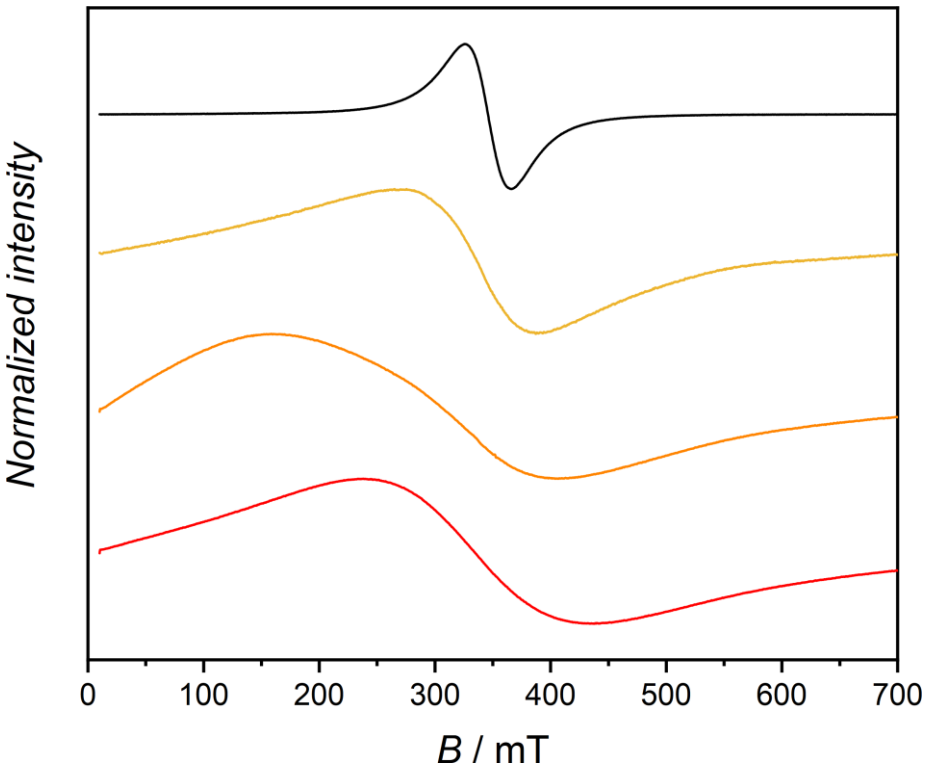

Figure S21. Comparison of X-band EPR spectra for **1Mn·8H$_2$O** (black line), **1Mn·3H$_2$O** (yellow line), **1Mn·2H$_2$O** (orange line) and **1Mn** (red line). All spectra were recorded at room temperature and normalized to [0,1].

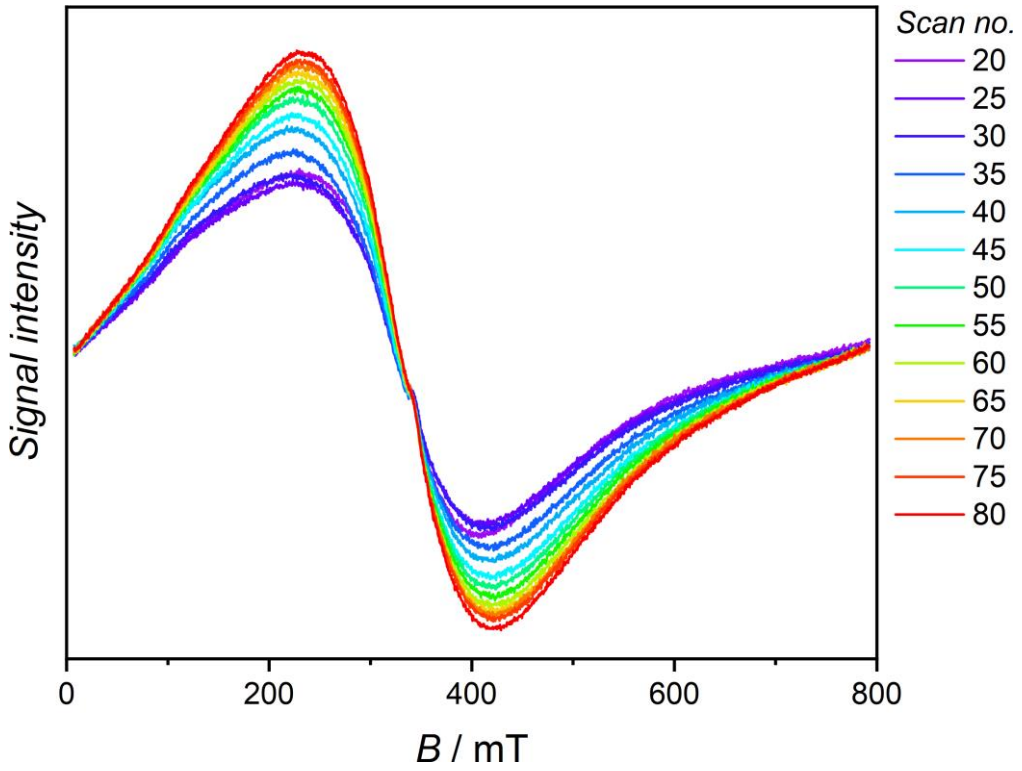

Figure S22. Comparison of scans 20-80 in the EPR dehydration experiment for **1Mn·8H$_2$O**, showing signal increase upon transition from **1Mn·2H$_2$O** to **1Mn**.

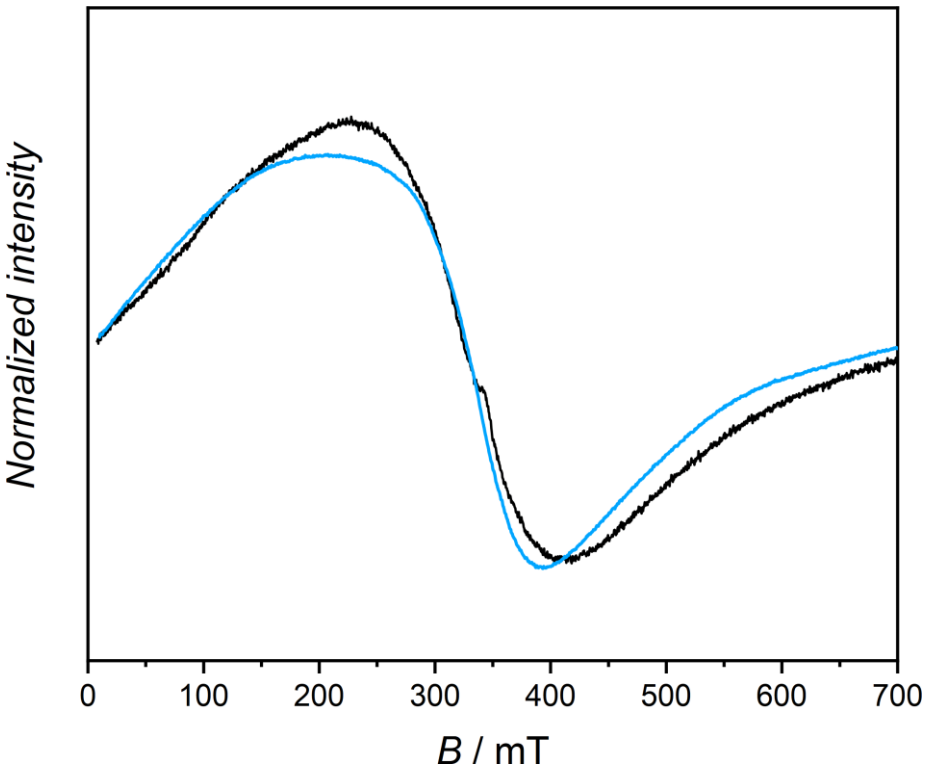

Figure S23. 25th scan of *in situ* EPR dehydration experiment (black line) compared with linear combination (1:1) of EPR spectra recorded for **1Mn·3H$_2$O** and **1Mn·2H$_2$O** (blue line).

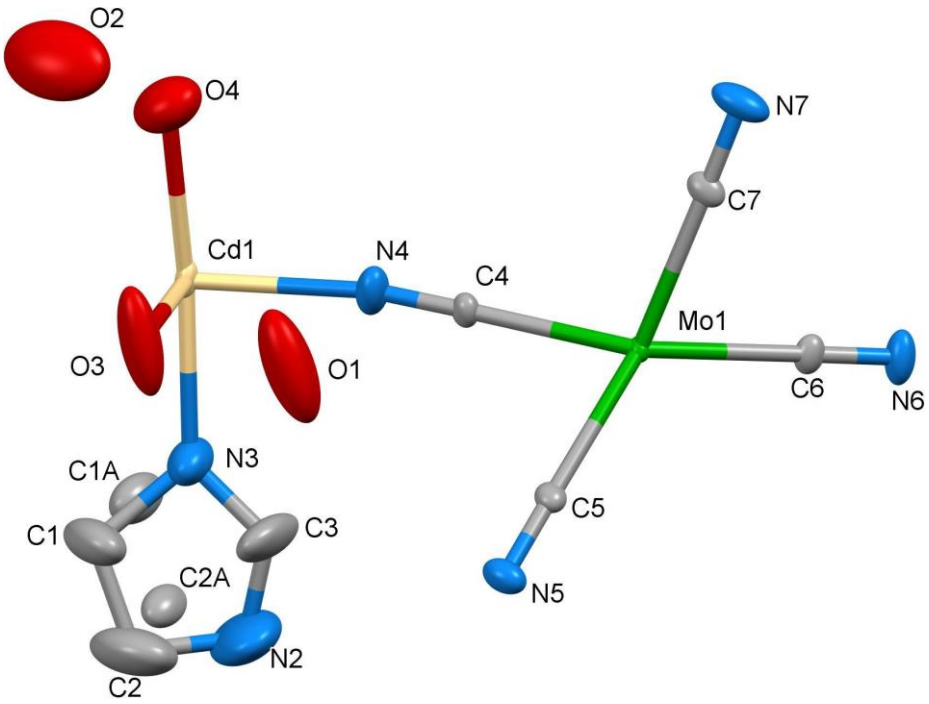

Figure S24. The asymmetric unit of **2Cd·8H$_2$O**. Centroids are depicted at the 50% probability level for a structure obtained at *T* = 100 K.

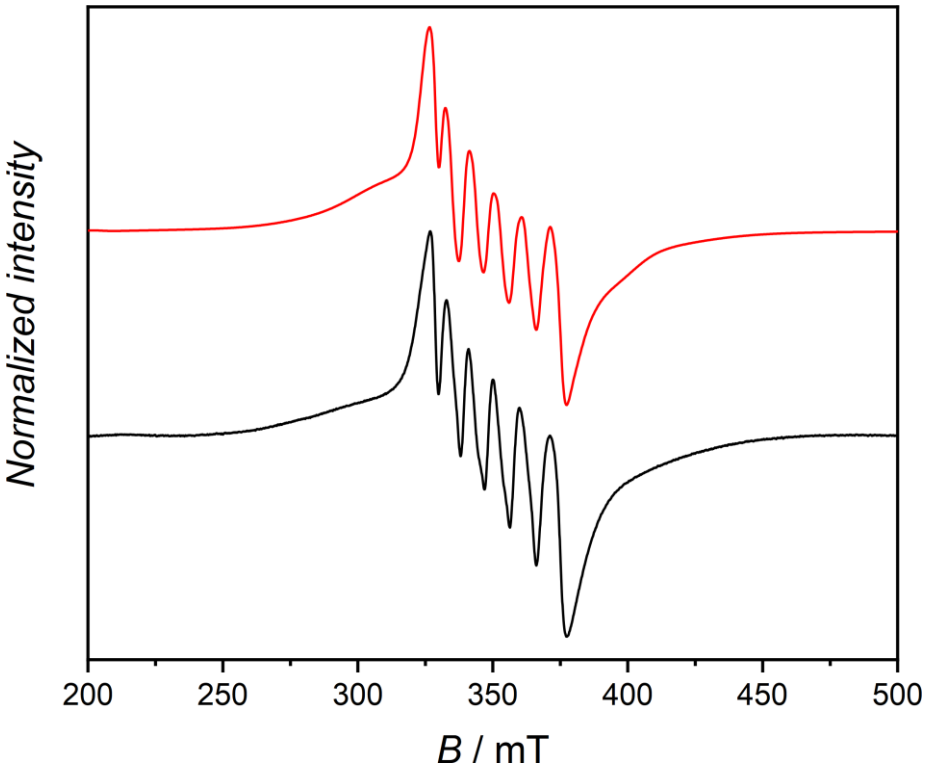

Figure S25. X-band (9.86 GHz) EPR spectrum of **2Cd·8H$_2$O:Mn** recorded at room temperature (black line) and simulated for *g* = 2.00, *D* = 0.02(2) cm^{-1} and *A* = 260 MHz (red line).

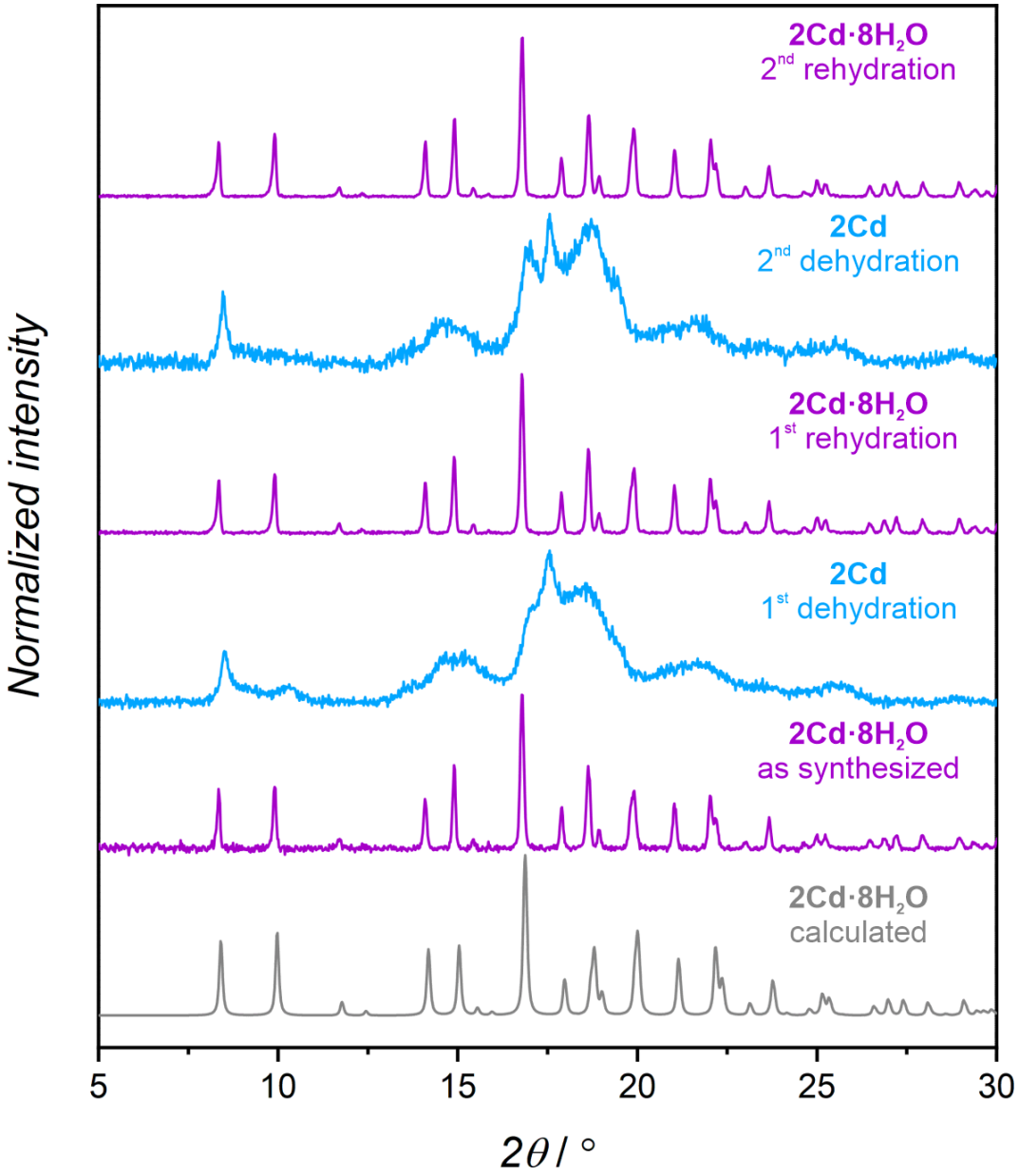

Figure S26. Powder X-ray diffraction patterns obtained for **2Cd·8H$_2$O** in two dehydration-rehydration cycles at room temperature and simulated from the single-crystal structure.

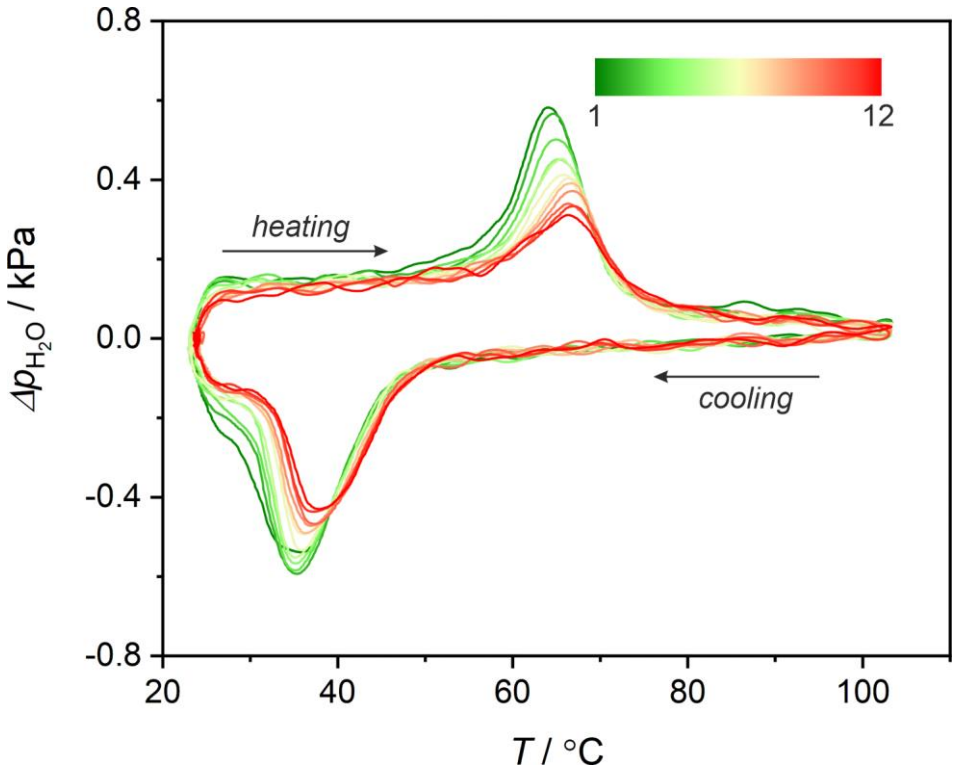

Figure S27. QE-TPDA profiles for **2Cd·8H$_2$O** obtained at a temperature sweep rate of 1.5 °C/min. using H_2O(2.4 kPa)/He mixture as a carrier gas.

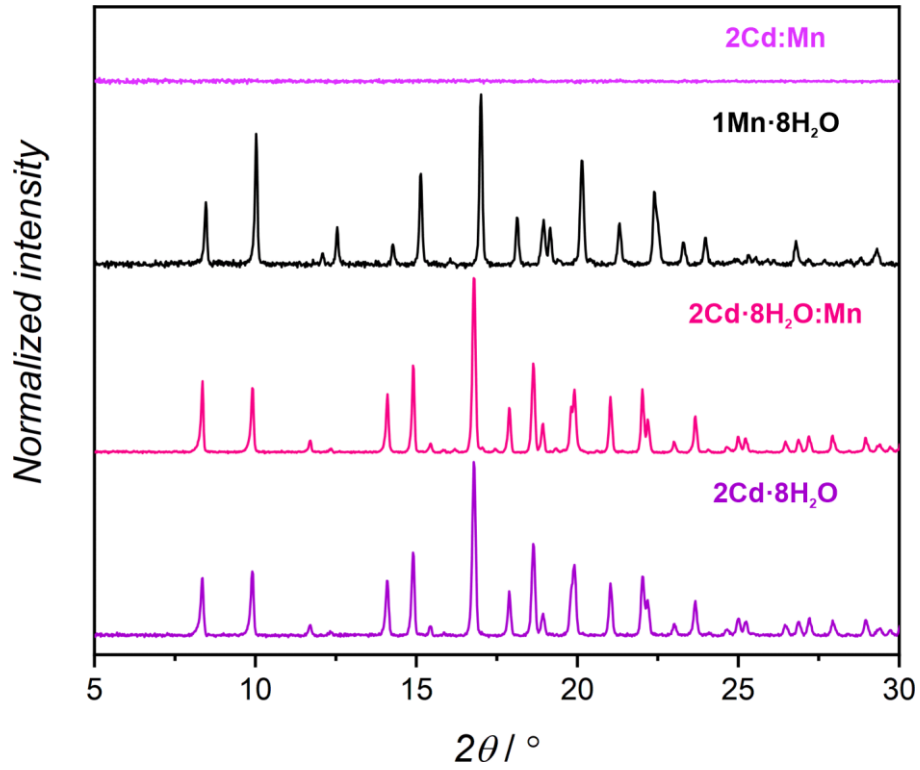

Figure S28. Comparison of powder X-ray diffraction patterns obtained for **1Mn·8H$_2$O**, **2Cd·8H$_2$O**, manganese(II)-doped cadmium compound **2Cd·8H$_2$O:Mn** and its dehydrated form.

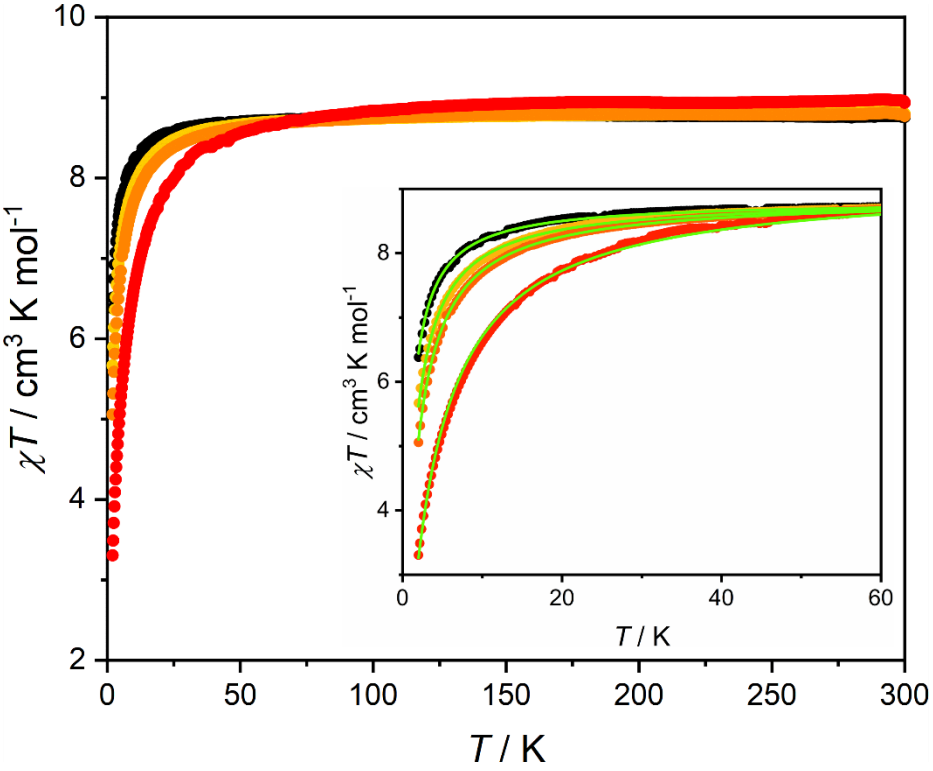

Figure S29. $\chi T(T)$ curves obtained for **1Mn·8H₂O** (black), **1Mn·3H₂O** (yellow), **1Mn·2H₂O** (orange) and **1Mn** (red) under H_{DC} = 0.1 T. Inset shows a close-up of 0-60 K range and Curie-Weiss fits (solid green lines).

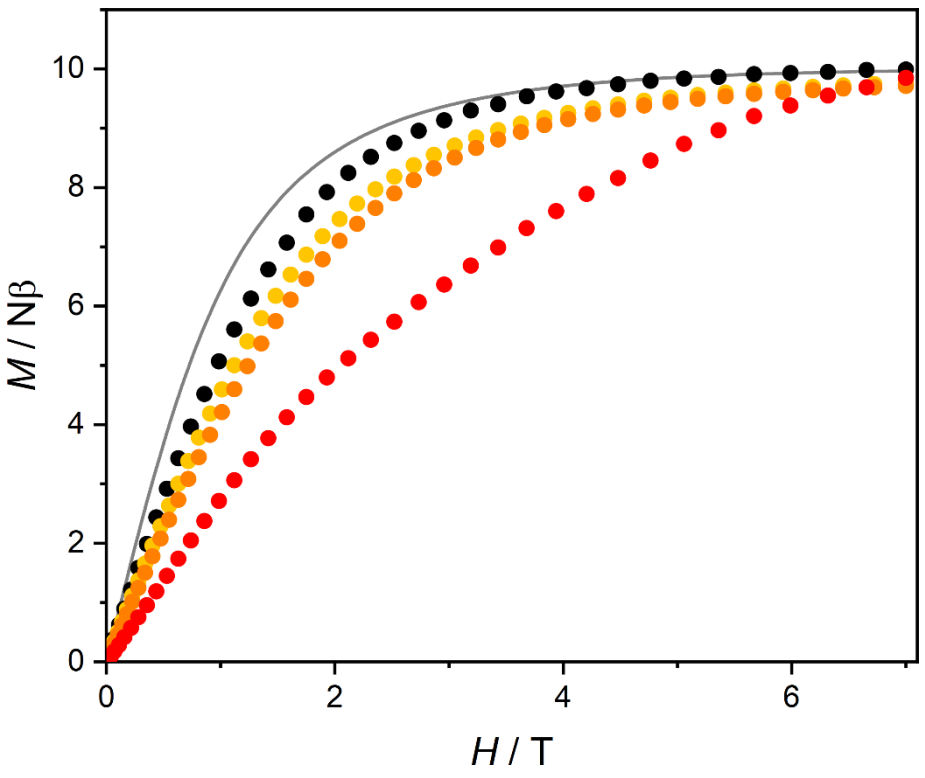

Figure S30. $M(H)$ curves obtained for **1Mn·8H₂O** (black), **1Mn·3H₂O** (yellow), **1Mn·2H₂O** (orange) and **1Mn** (red) at T = 2 K. Solid grey line shows the Brillouin function for two isolated S = 5/2 and g = 2.0.

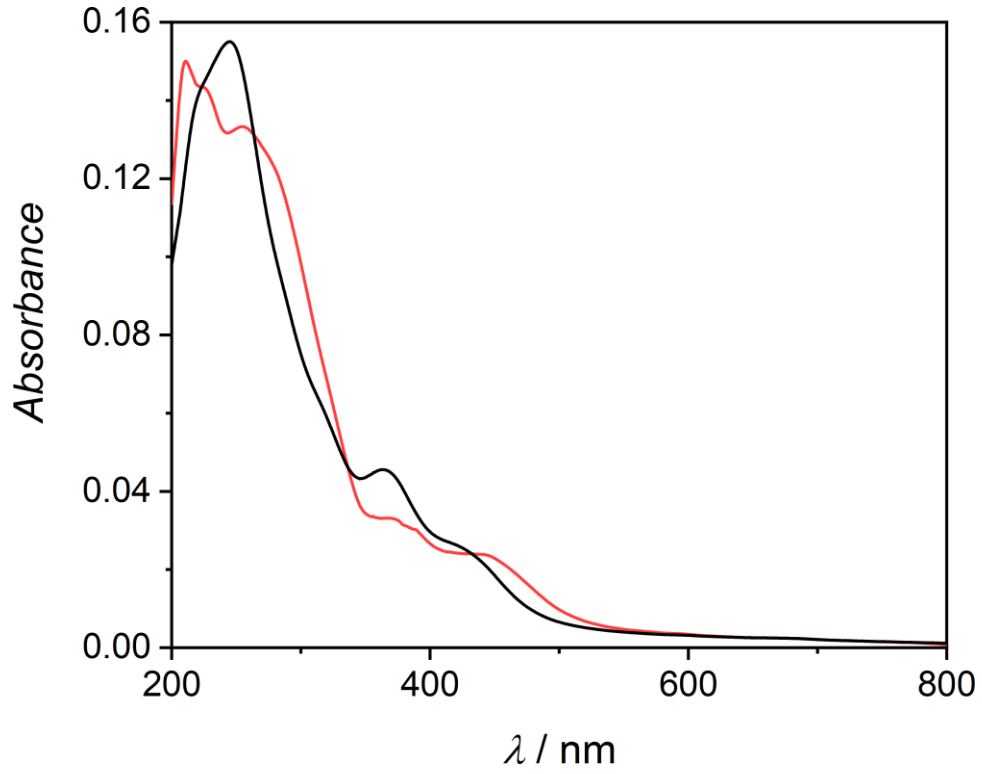

Figure S31. Solid state UV-Vis spectra for **1Mn·8H$_2$O** (black) and **1Mn** (red) at room temperature.

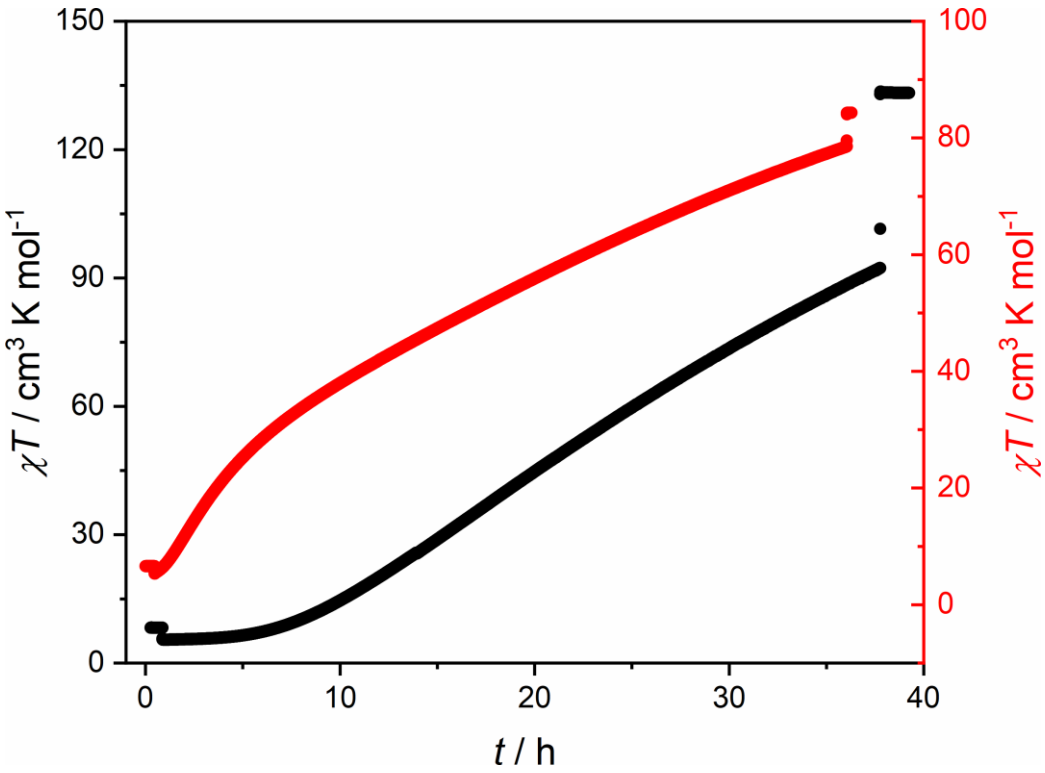

Figure S32. $\chi T(t)$ curves obtained for **1Mn·8H$_2$O** (black) and **1Mn** (red) upon 450 nm irradiation at T = 10 K and H_{DC} = 0.1 T.

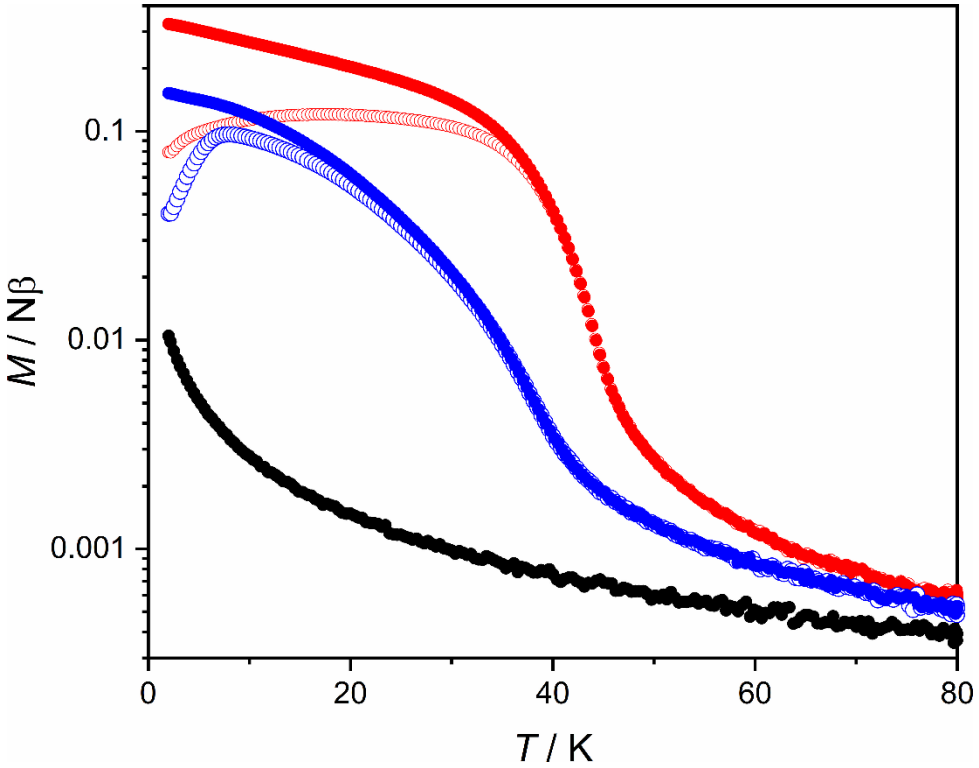

Figure S33. Field-cooled (closed symbols) and zero field-cooled (open symbols) curves for **1Mn·8H$_2$O** before irradiation (black), after 405 nm irradiation at 10 K (red) and after 2 hours of thermal relaxation at 240 K (blue); H_{DC} = 0.02 T.

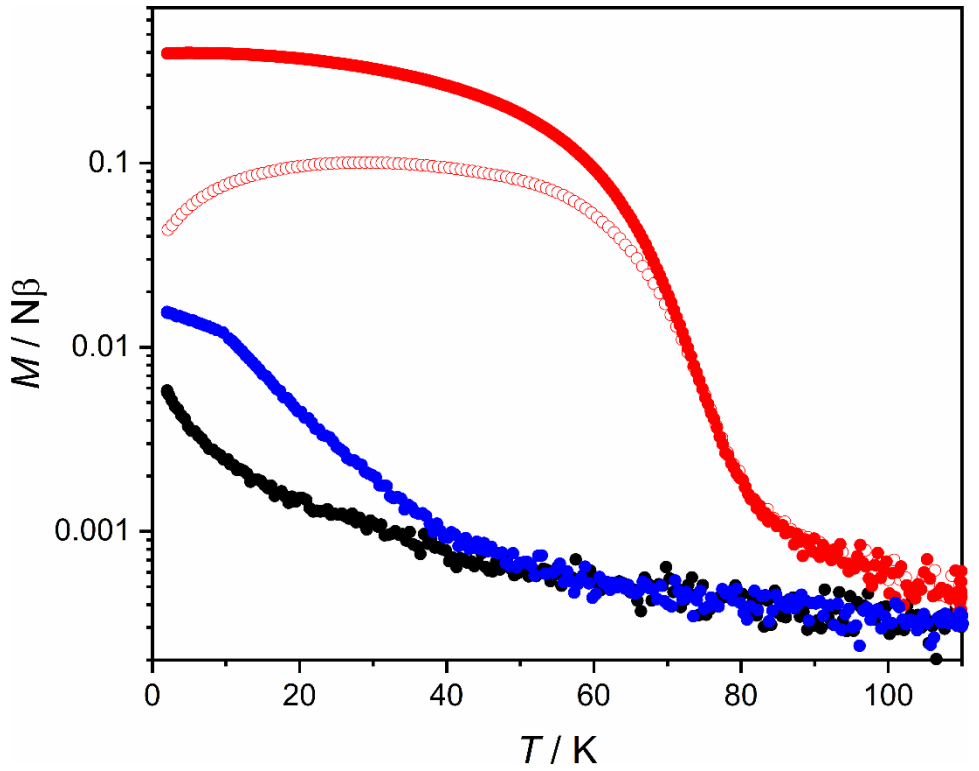

Figure S34. Field-cooled (closed symbols) and zero field-cooled (open symbols) curves for **1Mn** before irradiation (black), after 405 nm irradiation at 10 K (red) and after 1 hour of thermal relaxation at 315 K (blue); H_{DC} = 0.02 T.

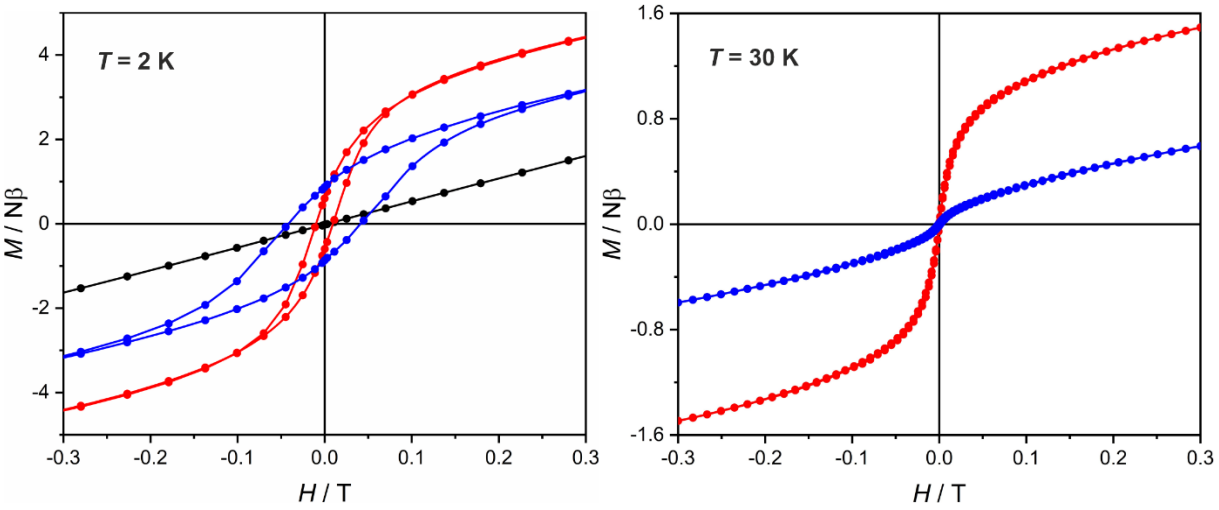

Figure S35. *M*(*H*) curves for **1Mn·8H$_2$O** before irradiation (black), after 405 nm irradiation at 10 K (red), and after 2 hours of thermal relaxation at 240 K (blue). Solid lines are guides for an eye.

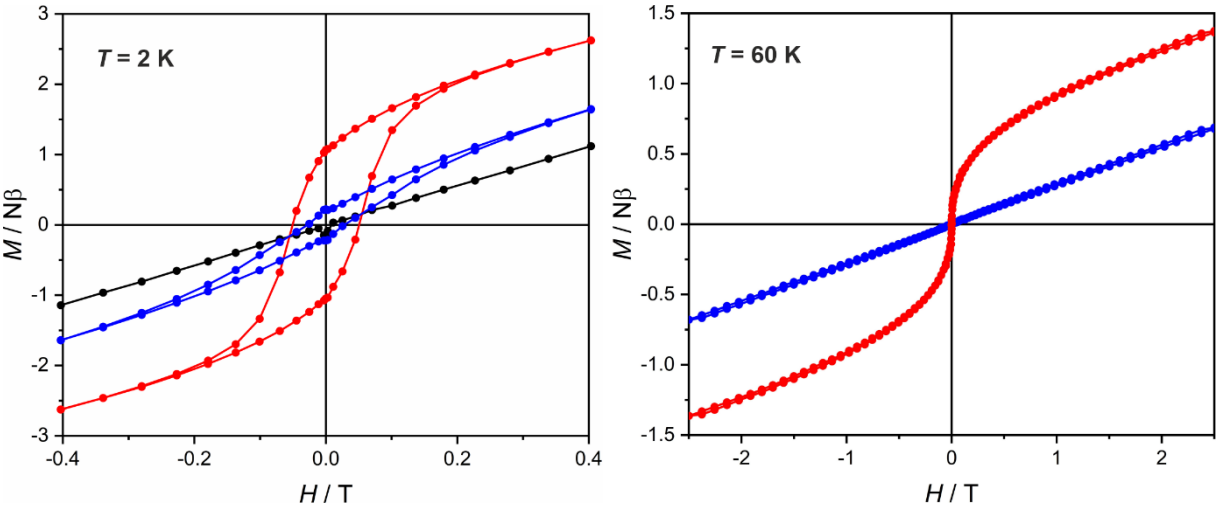

Figure S36. *M*(*H*) curves for **1Mn** before irradiation (black), after 405 nm irradiation at 10 K (red), and after 1 hour of thermal relaxation at 315 K (blue). Solid lines are guides for an eye.

Table S1. Crystallographic data obtained from SCXRD for **1Mn·8H$_2$O** and **2Cd·8H$_2$O**.

	1Mn·8H$_2$O	**2Cd·8H$_2$O**
CCDC deposition number	**2046137**	**2046138**
Formula	$C_{14}H_{16}Mn_2MoN_{12}O_8$	$C_{14}H_{20}Cd_2MoN_{12}O_8$
FW / g mol^{-1}	686.21	805.16
Temperature / K	295(2)	100(2)
Crystal system	monoclinic	monoclinic
Space group	*C*2/*c*	*C*2/*c*
a / Å	15.649(2)	15.8209(11)
b / Å	14.575(2)	14.7258(9)
c / Å	12.307(2)	12.4024(7)
β / °	108.364(6)	108.213(2)
V / Å^3	2663.9(6)	2744.7(3)
Z	4	4
ρ_{calc} / g cm^3	1.711	1.948
Abs. coeff / mm^{-1}	1.46	2.04
F(000)	1360	1560
Crystal size / mm	0.47 x 0.08 x 0.08	0.24 x 0.05 x 0.03
ϑ range / °	2.8–27.2	2.7-27.5
Reflections collected	9737	15248
R_{int}	0.046	0.041
Parameters/restraints	199/9	205/27
GOF on F^2	1.05	1.06
R_1 (refl. with I > 2σ(I))	0.042	0.036
wR_2 (all reflections)	0.101	0.083
Largest diff. peak and hole / e Å^{-3}	1.13/-0.89	2.30/-1.88

Table S2. Crystallographic data obtained from PXRD for **1Mn**, **1Mn·2H$_2$O** and **1Mn·3H$_2$O**.

	1Mn	**1Mn·2H$_2$O**	**1Mn·3H$_2$O**
CCDC deposition number	**2048779**	**2048780**	**2048781**
Formula	$C_{14}H_8Mn_2MoN_{12}$	$C_{14}H_8Mn_2MoN_{12}O_2$	$C_{14}H_8Mn_2MoN_{12}O_3$
FW / g mol^{-1}	550.14	582.14	598.14
Temperature / K	293(2)	293(2)	293(2)
Crystal system	triclinic	monoclinic	triniclinic
Space group	$P\bar{1}$	$C2/c$	$P\bar{1}$
a / Å	9.8543(5)	16.4048(6)	10.4152(6)
b / Å	10.0005(5)	12.9596(6)	10.4382(6)
c / Å	10.8395(6)	12.1716(5)	12.0481(8)
α / °	95.383(10)	90	74.301(4)
β / °	103.956(9)	119.340(2)	67.315(3)
γ / °	103.284(6)	90	75.015(4)
V / Å^3	996.3(1)	2255.7(2)	1145.7(1)
Z	2	4	2
ρ_{calc} / g cm^3	1.834	1.714	1.734
Abs. coeff / mm^{-1}	15.486	13.787	13.625
F(000)	536	1136	584
2ϑ range / °	6.98-40.03	7.01-40.00	7.01-40.00
GOF	0.41	0.78	0.57
R_p	0.0455	0.0875	0.0769
R_{wp}	0.0519	0.0976	0.0837

Table S3. Water adsorption isotherm data recorded for **1Mn** and data obtained by interpolation of water adsorption isotherm recorded at 313 K to water loadings corresponding to the experimental points at 298 K.

p_{298K} / kPa	m/m_0 (298 K) / %	p_{313K} / kPa	m/m_0 (313 K) / %	p_{313K} / kPa [313 K data interpolated to m/m_0 (298 K)]
0.14736	1.50612	0.44568	0.45834	0.51268
0.20719	3.40586	0.58098	2.57418	0.66000
0.26410	4.48121	0.71057	3.93808	0.82056
0.32628	5.21663	0.88261	4.78759	1.00725
0.38890	5.58731	1.02372	5.27333	1.18633
0.45101	6.37377	1.20635	5.62597	1.43031
0.51534	8.40742	1.39538	5.97376	1.73200
0.5798	9.03000	1.57838	8.06909	1.94358
0.64445	15.20212	1.86292	8.69576	2.57883
0.70738	18.23667	1.95611	9.08191	2.73031
0.77292	21.24157	2.28752	9.63624	3.15300
0.84219	21.93095	2.62215	16.02966	3.46848
0.90513	22.28711	2.82341	20.13623	3.66673
0.97174	22.62985	3.01007	20.87690	3.90032
1.03766	22.90689	3.16946	21.28357	4.08659
1.10199	23.07982	3.28978	21.57999	4.23255
1.16423	23.23948	3.42980	21.85340	4.39588
1.22951	23.37729	3.55193	22.09831	4.52287
1.29333	23.51214	3.69875	22.33977	4.68102
1.35424	23.63372	3.87106	22.58327	4.83306
1.41756	23.74984	4.02692	22.83146	4.96766
1.48303	23.85941	4.19601	23.04521	5.10449
1.54495	23.95836	4.36315	23.20352	5.24357
1.60554	24.05793	4.51578	23.37123	5.33887
1.67038	24.16001	4.66861	23.50214	5.55476
1.73287	24.24600	4.77779	23.59014	5.73369
1.79720	24.34308	4.92614	23.70711	5.88037
1.86141	24.43298	5.01409	23.79762	5.97378
1.92225	24.52163	5.14171	23.88484	6.09734
1.98677	24.59951	5.25800	23.96878	6.19786
2.05402	24.67630	5.33952	24.05866	6.26125
2.11727	24.78524	5.51755	24.14212	6.34426
2.18407	24.94272	5.74398	24.25095	6.47738
2.24486	25.03200	5.88015	24.34287	6.55459
2.3102	25.11144	6.02252	24.47989	6.63650
2.37212	25.18261	6.16452	24.55912	6.71901
2.43487	25.24348	6.26288	24.67829	6.7878
2.49514	25.28624	6.32716	24.75846	6.83516
2.5596	25.31683	6.39186	24.85977	6.86741
2.62368	25.37161	6.49874	24.96344	6.93612
2.69346	25.41797	6.57591	25.05817	7.01038
2.75551	25.46354	6.65179	25.12488	7.08340
2.81762	25.51754	6.74169	25.20208	7.16992
2.87454	25.57076	6.83030	25.28163	7.25519
2.94026	25.61509	6.90409	25.35162	7.32620
2.99959	25.67627	7.00595	25.41520	7.42422